

Tuning Charge-Separated State Lifetimes in Perovskite Nanocrystal-Perylenediimide Hybrids

Alejandro Cortés-Villena, José Garcés-Garcés, Alejandro Cadranel, Alberto García-Ros, Ángela Sastre-Santos, Fernando Fernández-Lázaro,* Julia Pérez-Prieto,* Dirk M. Guldi,* and Raquel E. Galian*

To surface engineer $CsPbBr_3$ nanocrystals (NCs), the use of functional perylenediimides (PDIs) featuring carboxylic acids of different spacer lengths afforded hybrid materials such as NC@PDI-Ph (phenyl spacer) and NC@PDI-PhPr (phenylpropyl spacer). Properties that are not seen by the individual components, are investigated by an arsenal of steady-state and time-resolved techniques. These ranged from photoluminescence (PL) to ultrafast transient absorption spectroscopy (TAS) combined with global target analyses. Herein, charge separation from NCs to the electron-accepting PDIs upon photoexcitation of either the NC or PDI unities is evidenced. Remarkable is not only the lifetime of the charge carriers, which is on the time scale of microseconds, that is, 34 and 63 μ s for NC@PDI-Ph and NC@PDI-PhPr, respectively, but also the control over their lifetimes through tuning phenylversus phenylpropyl-spacer length. These findings are of relevance to solar energy conversion, in general, and perovskite-based devices, in particular.

1. Introduction

Currently, colloidal all-inorganic lead-halide perovskite nanocrystals (NCs) are in the research spotlight. Their great light-harvesting capabilities, high photoluminescence quantum yields ($\Phi_{\rm PL}$), tunable bandgaps, long charge carrier diffusion lengths,

high surface-to-volume ratios, and solution processability, among others, make them particularly appealing. All of it renders them promising candidates for applications ranging from photovoltaics to photocatalysis.^[1]

As colloidal nanomaterials, precise control over their surface chemistry of perovskite nanocrystals is imperative for handling their optical properties, solubility, and stability.^[2] The use of oleic acid (OA) and oleylamine (OAm) ligand pairs ensures high-quality nanocrystals with excellent dispersibility.^[3] However, the insulating nature of the long-chain organic ligands limits charge transport properties. While their removal can enhance electronic properties, it can impact the overall colloidal stability.^[4] In terms of light emission, the fast radiative recombination rate of photoexcited NCs,

typically on the order of a few nanoseconds, restrains their effectiveness as an energy source. [3] Nevertheless, interfacing NCs with strong electron donors and/or acceptors offers an effective approach to funnel exciton energy in the form of separated electron and hole charge carriers. Interfacial charge transfer (CT) not only suppresses radiative recombination but also generates

A. Cortés-Villena, J. Pérez-Prieto, R. E. Galian Institute of Molecular Science University of Valencia c/Catedrático José Beltrán Martínez 2, Paterna, Valencia 46980, Spain E-mail: julia.perez@uv.es; raquel.galian@uv.es

J. Garcés-Garcés, A. García-Ros, Á. Sastre-Santos, F. Fernández-Lázaro Area of Organic Chemistry Institute of Bioengineering Miguel Hernández University Avda. Universidad S/N, Elche 03202, Spain E-mail: fdofdez@umh.es

= TI ODCID: I ::C

The ORCID identification number(s) for the author(s) of this article can be found under https://doi.org/10.1002/adom.202501175

© 2025 The Author(s). Advanced Optical Materials published by Wiley-VCH GmbH. This is an open access article under the terms of the Creative Commons Attribution-NonCommercial License, which permits use, distribution and reproduction in any medium, provided the original work is properly cited and is not used for commercial purposes.

DOI: 10.1002/adom.202501175

A. Cadranel, D. M. Guldi

FAU Profile Center Solar Department of Chemistry and Pharmacy & Interdisciplinary Center for Molecular Materials (ICMM) Friedrich-Alexander-Universität Erlangen-Nürnberg (FAU) Egerlandstrasse 3, 91058 Erlangen, Germany

E-mail: dirk.guldi@fau.de

A. Cadranel

CONICET – Instituto de Química Física de Materiales Medio Ambiente y Energía (IN-QUIMAE) Universidad de Buenos Aires Viamonte 430, Buenos Aires 1053, Argentina

A. Cadranel Facultad de Ci

Facultad de Ciencias Exactas y Naturales Departamento de Química Inorgánica Analítica y Química Física Universidad de Buenos Aires

Viamonte 430, Buenos Aires 1053, Argentina



www.advopticalmat.de

long-lived charge carriers, thereby enhancing the potential for optoelectronics and energy conversion applications.^[5] In turn, CT across nanoscale semiconductor interfaces following photoexcitation is a hot topic. In this regard, Wu et al.[6] explored, for example, the electron and hole transfer dynamics from CsPbBr₃ NCs to benzoquinone (BQ) and phenothiazine (PTZ), respectively. This pioneering study inspired several studies involving a variety of organic electron acceptors and donors.^[7] Most of them lacked, however, an unambiguous corroboration for the formation of the respective one-electron oxidized electron donor or reduced electron acceptor by spectroscopic methods. Dynamics and quantum yields of interfacial CTs are proportional to the electronic coupling between the surface-anchored electron donors and/or acceptors. Important is hereby the optimization of the orbital overlap through a change in interfacial distance. [7ab] Hereby, changing the spacer stands out and is typically done by using conventional chalcogenide quantum dots.^[8] But, the alkyl chain length of the spacer is decisive in terms of the trade-off between charge separation and recombination.[9]

Perylenediimides (PDIs) have widely been used as visible-light absorbing electron acceptors in organic electronics and photovoltaics. [10] Their versatility stems from tunable electronic features. For instance, substitutions at the imide nitrogen enhance solubility and influence solid-state packing, on the one hand, whereas modifications at the bay/ortho positions allow fine-tuning of electron affinity and optical absorption, on the other hand. Together, these structural variations enable precise control over the functional behavior of PDIs in optoelectronic applications. [11]

Given their strong electron-accepting character,[12] integrating PDIs onto NCs is an advanced strategy en-route toward long exciton lifetimes. Up to now, to the best of our knowledge, only a limited number of examples have been reported. Rossi et al.[13] studied non-confined CsPbBr3 NCs as energy donor and two carboxylfunctionalized PDIs as energy acceptors. Time-correlated single photon counting (TCSPC) measurements revealed an amplified PDI fluorescence stemming from a Förster-resonance energy-transfer (FRET). It was shown to go hand-in-hand with a 65% and 45% NC emission quenching for the most electrondeficient and the less electron-deficient energy acceptors, respectively. Similarly, Kubo et al. investigated the interactions between confined CsPbBr₃ NC energy donors and two different PDI energy acceptors, namely, PBI1 (monodentate perylenebisimide) and PBI2 (bidentate perylenebisimide).[14] A PDI fluorescence enhancement in NC@PBI1 was evident, while a PBI2 fluorescence quenching NC@PBI2 was observed. Strong π - π interactions arising from the PBI2 self-assembly on the perovskite surface was given as a rationale. A charge transfer rather than energy transfer was reported by Gélvez-Rueda between quasi-2D CsPbBr3 NPLs (4 layers) and PDIs to afford NPL+-PDIcharge-separated states (CSS) employing ultrafast techniques.^[15] Depending on photoexciting either the CsPbBr₃ NPLs or PDIs, differences in the charge separation but not in the charge recombination kinetics were noted. More recently, charge transfer rate constants have been tuned by adjusting the driving forces between the thickness-controlled quantum confinement in CsPbBr₂ NPLs and electron accepting strength in PDIs, specifically comparing perylene monoimide diester (PMIDE) versus perylene diimide (PDI).[16] Investigations into the effect of the spacer length between the organic molecules and the NCs are still lacking in the field of perovskite NCs. This is where the present work truly stands out.

Herein, we probe unidirectional charge transfer dynamics, specifically, charge separation and recombination, from quantum-confined CsPbBr3 NCs to electron-accepting PDIs featuring phenyl- and phenylpropyl-spacers in NC@PDI-Ph and NC@PDI-PhPr hybrids, respectively. We observed spacerdependent excited-state deactivation that differs from previous works.[13,14] Through the combination of steady-state and timeresolved photoluminescence (PL), ultrafast transient absorption (TA) spectroscopies, and global target analyses, we corroborated unidirectional charge separation evolving from NCs to both PDIs, regardless of whether NCs or PDIs were photoexcited. In our analysis, several charge-separated species were detected, which ultimately charge recombine in the microsecond time regime. Charge recombination was hereby slower when a phenylpropyl-spacer rather than a phenyl-spacer was used. This work builds upon the findings reported in recent literature and significantly extends it,[15,16] by introducing a modular strategy to obtain exceptionally long-lived charge-separated states (CSSs), that is, on the microsecond time scale. The use of 0D nanocrystals and perylenediimides (PDIs) with carboxylic acid anchors enhances the interactions with the nanocrystal surface, compared to 2D perovskite materials and previously used alkylammonium linkers. Such features are of great relevance for charge extraction efficiencies in future perovskite-based devices.

2. Results and Discussion

2.1. Formation of Perovskite Nanocrystal-Perylenediimide Hybrids and Steady-State Optical Features

Colloidal cubic-shaped CsPbBr $_3$ perovskite nanocrystals (NCs) (Figure 1a) were synthesized through a previously reported hotinjection approach with an average nanocrystal edge-to-edge length of 6.1 \pm 0.7 nm (Figure S1, Supporting Information). [3,17] Oleic acid (OA) and oleylamine (OAm) were used as organic ligands to passivate the NC surface. CsPbBr $_3$ NCs were effectively utilized as electron donors in both the ground and excited states (vide infra). As electron acceptors, two asymmetrically substituted PDIs (Figure 1a) with phenyl- and phenylpropyl-spacers linking the carboxylic acid anchors to the PDI core were used.

They have been synthesized in a one-step statistical condensation reaction between tetrachloroperylene bisanhydride and equimolar quantities of the corresponding anilines (Scheme S1, Supporting Information).^[18] From here on, PDI-Ph and PDI-PhPr will refer to PDIs with phenyl- and phenylpropyl-spacers, respectively. Both PDIs were fully characterized by nuclear magnetic resonance techniques such as ¹H-NMR (Figures S2 and S3, Supporting Information), ¹³C-NMR (Figures S4 and S5, Supporting Information), COSY (Figures S6 and S7, Supporting Information), and high-resolution Mass Spectrometry HR-MALDI-ToF (Figures S8 and S9, Supporting Information).

Steady-state absorption and emission spectra of NC (0.05 μ M), PDI-Ph (1.5 μ M), and PDI-PhPr (1.5 μ M) in toluene are shown in Figure S10 (Supporting Information). The NC exhibited an exciton peak at 496 nm and a narrow PL maximum at 503 nm under 365 nm photoexcitation, consistent with a weak

21951071, 2025, 28, Downloaded from https://advanced.onlinelibrary.wiley.com/doi/10.1002/adom.202501175 by Universidad Miguel Hernández De Elche, Wiley Online Library on [15/10/2025]. See the Terms

s (https://onlinelibrary.wiley.com/terms-and-conditions) on Wiley Online Library for rules of use; OA articles are governed by the applicable Creative Commons I

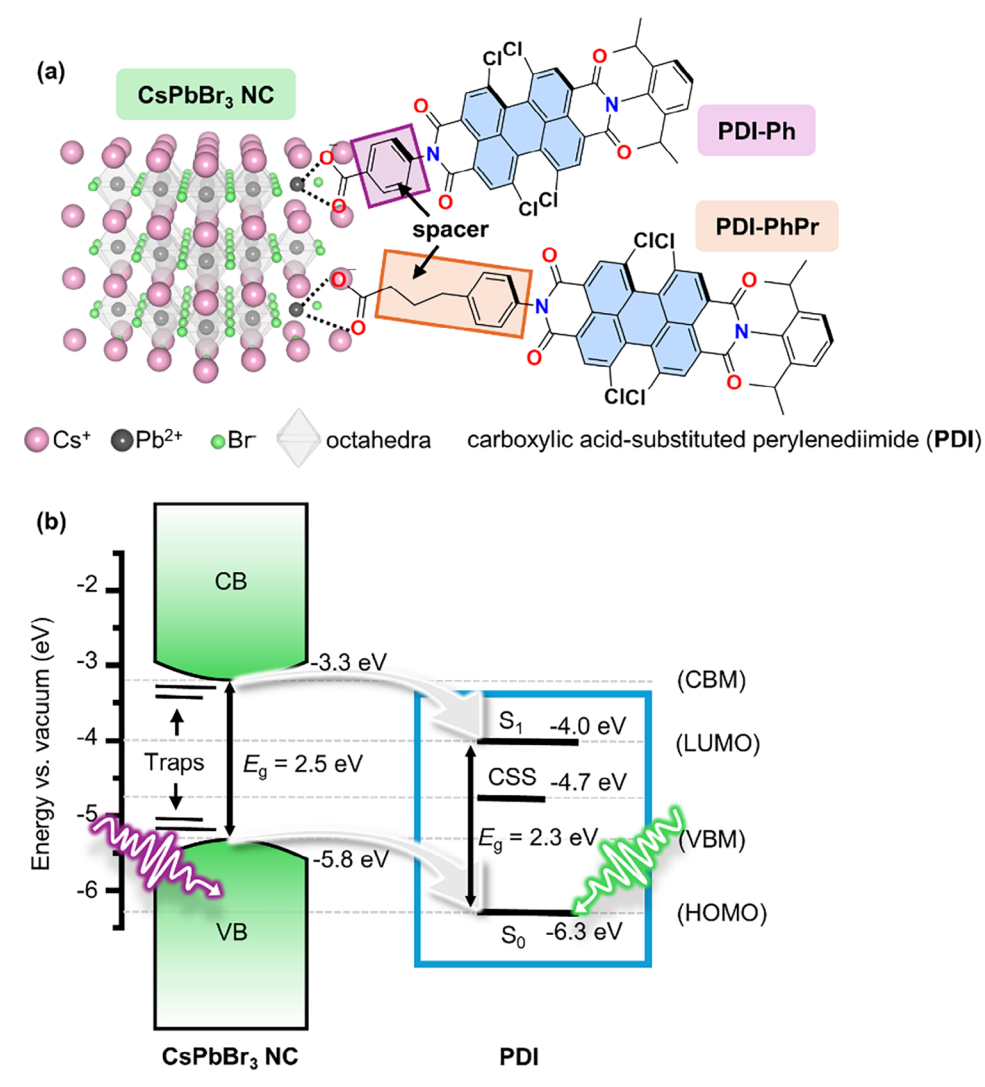


Figure 1. a) Crystalline structure of the CsPbBr₃ NC and molecular structures of PDI-Ph and PDI-PhPr interacting with the NC surface (OA/OAm are omitted for the sake of clarity). b) Energy level alignment between the NC and PDI against vacuum, highlighting that selective photoexcitation of both systems yields charge-separated states (CSSs).

quantum-confinement regime and the monodisperse nature determined by Transmission electron microscopy (TEM) analyses. [17] The Φ_{PL} of the NC is moderate (53%) and suggests the presence of trap states that facilitate non-radiative recombination pathways. For both PDI-Ph and PDI-PhPr, the main absorptions at 490 and 523 nm are assigned to 0–1 and 0–0 vibronic transitions, respectively, corresponding to the singlet ground state (S₀) to the first singlet excited state (S₁). Their fluorescence spectra exhibit a maximum at 553 nm with a shoulder at 600 nm. The Φ_{PL} of PDI-Ph and PDI-PhPr are similarly high (85–95%). These results support the notion that imide substituents exert only a subtle influence on the optical properties of PDIs. [19]

Combining oleate-passivated **NC**s with an excess of electron-accepting **PDI**s bearing carboxylic acid anchors enables the partial replacement of oleates with **PDI-Ph** and **PDI-PhPr**.^[15,20] Binding of the carboxylic acid group of oleic acid (OA) to the perovskite surface–primarily lead cations–is rather weak and, there-

fore, highly dynamic in nature. [4a] This facilitates ligand exchange processes at the NC surface resulting in effective functionalization. To this end, NC@PDIs hybrids were prepared by titrating increasing PDI concentrations (0, 0.25, 0.5, 0.75, 1, and 1.5 μ M) into constant NC concentrations (0.05 μ M) up to a maximum PDI-to-NC ratio of 30:1.[21] As PDI concentrations increase, PDI absorption features emerge in the absorption spectrum (Figure 2a,b). A comparison between PDI-Ph and PDI-PhPr in toluene indicates i) a change in the absorption ratio (A₀₋₀/A₀₋₁), ii) a blueshift of the two absorption peaks, and iii) an absorption tail in the 530–650 nm range (Figure S11, Supporting Information).

Optical and electrochemical data (Figure S12, Supporting Information) for PDI-Ph and PDI-PhPr, as well as the energy levels for the NC, are taken from the literature, ^[17] to construct the energy level alignment that is shown in Figure 1b. Selective NC photoexcitation at 365 nm is expected to result in a charge separation by transferring an electron from the NC conduction band minimum (CBM) to the lowest-unoccupied molecular orbital (LUMO)

21951071, 2025, 28, Downloaded from https://advanced

onlinelibrary.wiley.com/doi/10.1002/adom.202501175 by Universidad Miguel Hernández De Elche, Wiley Online Library on [15/10/2025]. See the Terms

itions) on Wiley Online Library for rules of use; OA articles are governed by the applicable Creative Commons

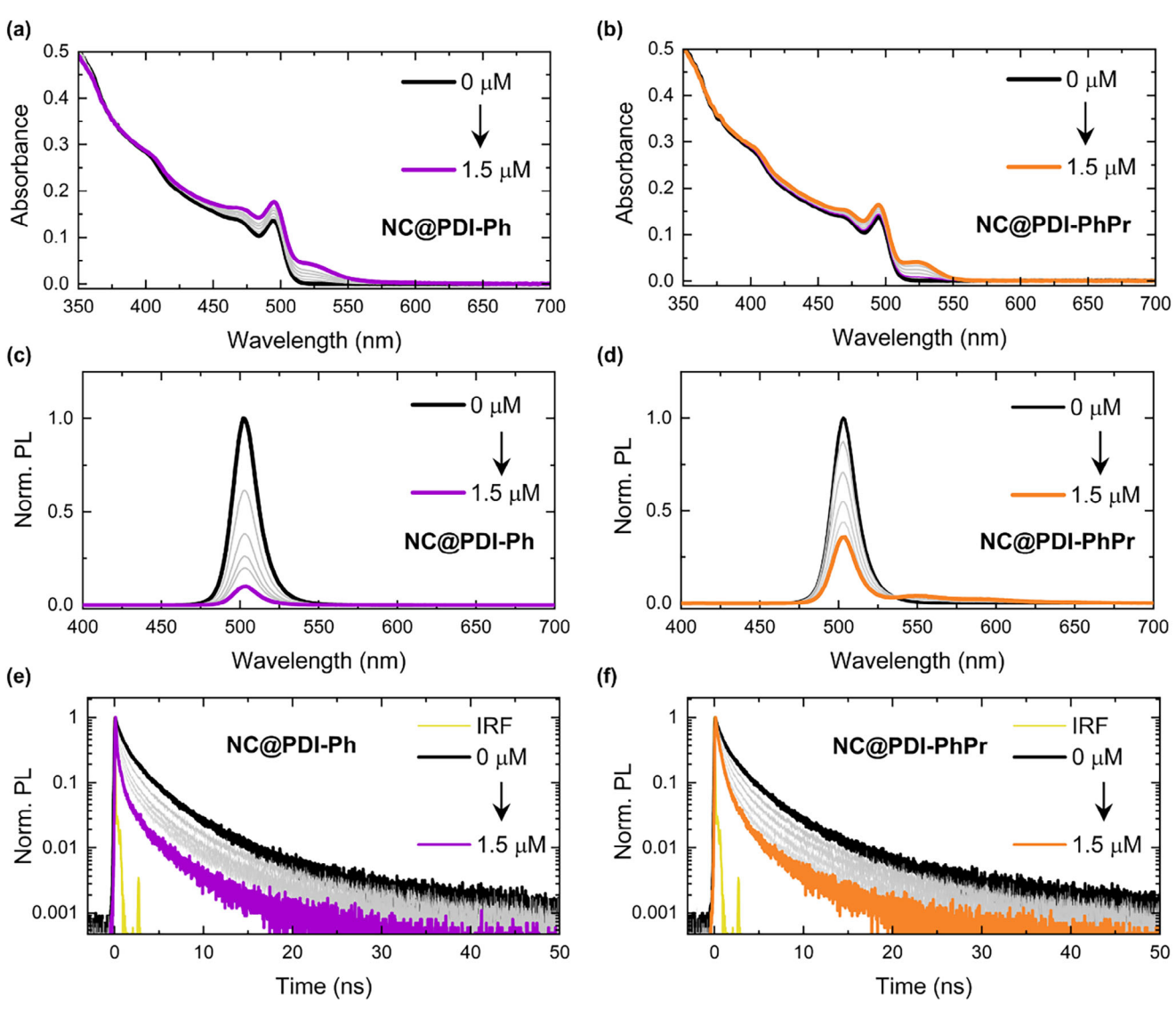


Figure 2. a) Absorption spectra of NC upon increasing PDI concentration in toluene for NC@PDI-Ph b) and NC@PDI-PhPr. Normalized PL spectra for NC@PDI-Ph c) and NC@PDI-PhPr d) under photoexcitation at 365 nm. Normalized PL kinetic traces for NC@PDI-Ph e) and NC@PDI-PhPr f) recorded at 503 nm under pulsed-laser photoexcitation at 375 nm.

of **PDI**, resulting in a (**NC****@**PDI****) CSS. Likewise, 525 nm photoexcitation of **PDI** forms the same (**NC****@**PDI****) CSS via an electron transfer from the **NC** valence band maximum (VBM) to the highest-occupied molecular orbital (HOMO) of the **PDI**. (**NC****@**PDI****) CSS presents an estimated energy of 1.6 eV.

2.2. Excited-State Interactions in Perovskite-Perylenediimide Hybrids

Steady-state and time-resolved PL experiments were conducted with the NC@PDIs dispersed in toluene. A strong attenuation of the PL intensity of the NC under selective 365 nm photoexcitation was observed in both systems (Figure 2c,d). Quenching efficiency (Φ_Q), calculated at a 30:1 ratio, was 90% and 64% for NC@PDI-Ph and NC@PDI-PhPr, respectively. In other words,

the shorter spacer in NC@PDI-Ph imposed a stronger quenching (Figure S13, Supporting Information). Analyses of a double-reciprocal plot of $(I_0-I)^{-1}$ versus $[PDI]^{-1}$ afforded apparent association constants (K_{app}): $(2.25\pm0.05)\times10^6~M^{-1}$ and $(0.31\pm0.07)\times10^6~M^{-1}$ for NC@PDI-Ph and NC@PDI-PhPr, respectively (Figure S14, Supporting Information). Notably, PDI-centered fluorescence remained discernible in NC@PDI-PhPr (Figure 2d), whereas it was completely absent in NC@PDI-Ph (Figure 2c). Lat this point, we postulate that charge separation evolving from the NC to PDI under 365 nm photoexcitation is the dominant mechanism for the excited-state quenching. A NC-to-PDI energy transfer pathway should not be ruled out, when considering the driving force ($\Delta G_{ET} = -0.2~eV$) and the spectral overlap integral ($J = 1.27 \times 10^{15}~nm^4~M^{-1}~cm^{-1}$) between the excited state donating NC emission and the excited state accepting PDI absorption (Figure S15, Supporting Information). However, the absence





www.advopticalmat.de

of NC absorptions in the photoluminescence excitation (PLE) spectrum of NC@PDI-Ph and NC@PDI-Phr speaks against an energy transfer scenario (Figure S16, Supporting Information), despite the large spectral overlap integral value. An energy transfer scenario due to unfavorable dipole orientations for a Förster mechanism and unfavorable orbital overlap for a Dexter mechanism is non-competitive relative to charge separation, probably due to the perpendicular orientation of PDI relative to the NC surface. Additionally, $\Phi_{\rm Q}$ fluorescence of PDIs at a ratio of 100:1 relative to NC was calculated under 525 nm photoexcitation to be 86% and 17% for NC@PDI-Ph and NC@PDI-PhPr, respectively (Figure S17, Supporting Information).

Independent confirmation for charge separation evolving from both **PDIs** to **NC** rather than fluorescence deactivation due to **PDI-Ph** aggregation, came from quenching assays of the **PDI-Ph** fluorescence in different mixed halide $CsPbCl_xBr_{3.x}$ -**PDI-Ph** (Figure S18a, Supporting Information). It is well known that the halide-alloying in perovskites affects the VBM position. [3,23] Therefore, the driving force (ΔG) for charge separation from the VBM of the **NC** to the HOMO level of **PDI-Ph** is expected to decrease upon chloride-alloying. This agrees with the decrease of quenching efficiency (Φ_Q) as a function of ΔG (Figure S18b, Supporting Information) and corroborates charge separation from the **NCs** to the **PDI-Ph** according to the energy-level alignment (Figure S18c, Supporting Information).

Time-resolved PL experiments by means of time-correlated single photon counting (TCSPC) were conducted to investigate the recombination dynamics of band-edge excitons in the NC (Figure 2e,f). Under 375 nm pulsed-laser excitation, the NC emission decay monitored at 503 nm resulted in 3 lifetimes: bright exciton components X1 [0.5 ns (22%)], X2 [2.9 ns (60%)], and X3 [13.2 ns (18%)], respectively. Upon **PDI** addition (ratio of 30:1), quenching of the time-resolved PL of NC was evident with the bright exciton lifetimes of 0.1 ns (36%), 0.8 ns (36%), 5.2 ns (28%) for NC@PDI-Ph and 0.3 ns (45%), 1.3 ns (40%), 7.3 ns (15%) for NC@PDI-PhPr. All lifetime parameters and their respective contributions are gathered in Table \$1 (Supporting Information). Accordingly, $\Phi_{\rm Q}$ (calculated from the fastest component X1) was 87% and 51% for NC@PDI-Ph and NC@PDI-PhPr, respectively,[24] consistent with the data obtained from steadystate PL.[25]

Attenuated total reflectance-Fourier transform infrared (ATR-FTIR) spectroscopy was carried out to confirm the formation of **NC@PDIs** (Figure S20, Supporting Information). The appearance of the C=O stretching band at 1712 cm⁻¹, characteristic of the free carboxylic acid group in OA, indicates a partial replacement of oleate by carboxylic acid-functionalized **PDI**.^[20] However, the presence of unbound oleate molecules mask the **PDI-Ph** signature. Based on control experiments with **PDI-CO**,^[25] high apparent association constant K_{app}, strong PL quenching-vide supra-and transient absorption data-vide infra-revealed that **NC@PDIs** were formed under these experimental conditions.

2.3. Probing Charge Separation in Perovskite Nanocrystal-Perylenediimide Hybrids

Femtosecond transient absorption spectroscopy (fs-TAS) was employed to assess the charge separa-

tion between NCs and surface-bound PDIs upon photoexcitation. [26] Two different pump excitation wavelengths, namely 365 and 525 nm, were used for the selective photoexcitation of PDIs and NCs, respectively. Initially, dynamics at low-energy 525 nm photoexcitation allowed identifying the kinetic components and was used, in a later step, as internal references to rationalize the analysis under high-energy 365 nm photoexcitation.

NC was photoexcited at 525 nm with an ultrafast laser pulse. Although NC failed to exhibit sizeable absorptions at 525 nm, as tested by steady-state absorption spectroscopy, control fs-TAS experiments on the NC display ground-state bleaching (GSB) of the exciton features (XB) in the 2D pseudocolor map (Figure S21, Supporting Information). Our observation is rationalized by considering the presence of sub-bandgap states, from which photocarriers are promoted into the conduction band, as was previously reported.[27] The two XBs at 475 and 498 nm, due to bandedge fillings effects of electrons and holes, are consistent with those observed in the steady-state absorption experiments. They are superimposed on an excited state absorption (ESA) feature at 513 nm. Responsible are interactions between hot and band-edge excitons and its decay is accompanied by the growth of XB features. Implicit are hot exciton relaxations. After exciton cooling, that is, from hot-down to band-edge states (<1 ps), the resulting XB features are superimposed on a broad ESA band between 450 and 520 nm.

Target analysis of the fs-TA included four species for the NC control: hot exciton (HX), biexciton (XX), and two exciton components (X1) and (X2), with lifetimes of 0.3 ps, 34 ps, 1.1 ns, and 4.8 ns, respectively. HX decays are essentially hidden within the time resolution of our experimental setup and is close to the coherent artefacts that are linked at the early times to the high pump-energy of 1 μJ , whereas XX is due to generation of biexcitons in the same nanocrystal.

Upon 365 nm photoexcitation (Figure S22, Supporting Information), the shape of the fs-TA resembled the one observed by us under similar pump fluence conditions.[24] Longer-lived HX is the first species, when compared to that of NC under 525 nm photoexcitation. It corresponds to HX with excitonic ESAs at 474, 496, and 513 nm and transitions into multiexcitons MXs and biexcitons XXs. Considering a high-energy fluence of 45 mJ cm⁻² and an estimated absorption cross-section of 1.7×10^{-14} cm² for similarly sized CsPbBr3 nanocrystals at 400 nm, the average exciton occupancy ($\langle N \rangle$) was calculated to be at least 1412. This clearly confirms the formation of multiexcitonic states in our experiments. HX, MX, and XX decay sequentially with lifetimes of 2, 6, and 24 ps, respectively. The X1 lifetime of 0.6 ns was consistent with that one observed via TCSPC. A single 4.3 ns lifetime was derived for the X2/X3 components, due to the 7 ns time window of our experimental setup.

PDI-Ph and PDI-PhPr references were also photoexcited at 525 nm. The 2D pseudocolor map of PDI-Ph (Figure 3a) displays typical GSBs at 490 and 523 nm, with the latter overlapping with the pump laser scattering, which was not considered in the analysis. Stimulated emission (SE) feature also appears at ≈550 nm, with a shoulder at 600 nm, consistent with the steady-state measurements. In addition, a broad ESA extending from 650 nm all the way into the near-Infrared (NIR) region was observed and attributed to the singlet excited state. Representative kinetic traces

21951071, 2025, 28, Downloaded from https://ad

/doi/10.1002/adom.202501175 by Universidad Miguel Hernández De Elche, Wiley Online Library on [15/10/2025]. See the Term

on Wiley Online Library for rules of use; OA articles are governed by the applicable Creative Commons

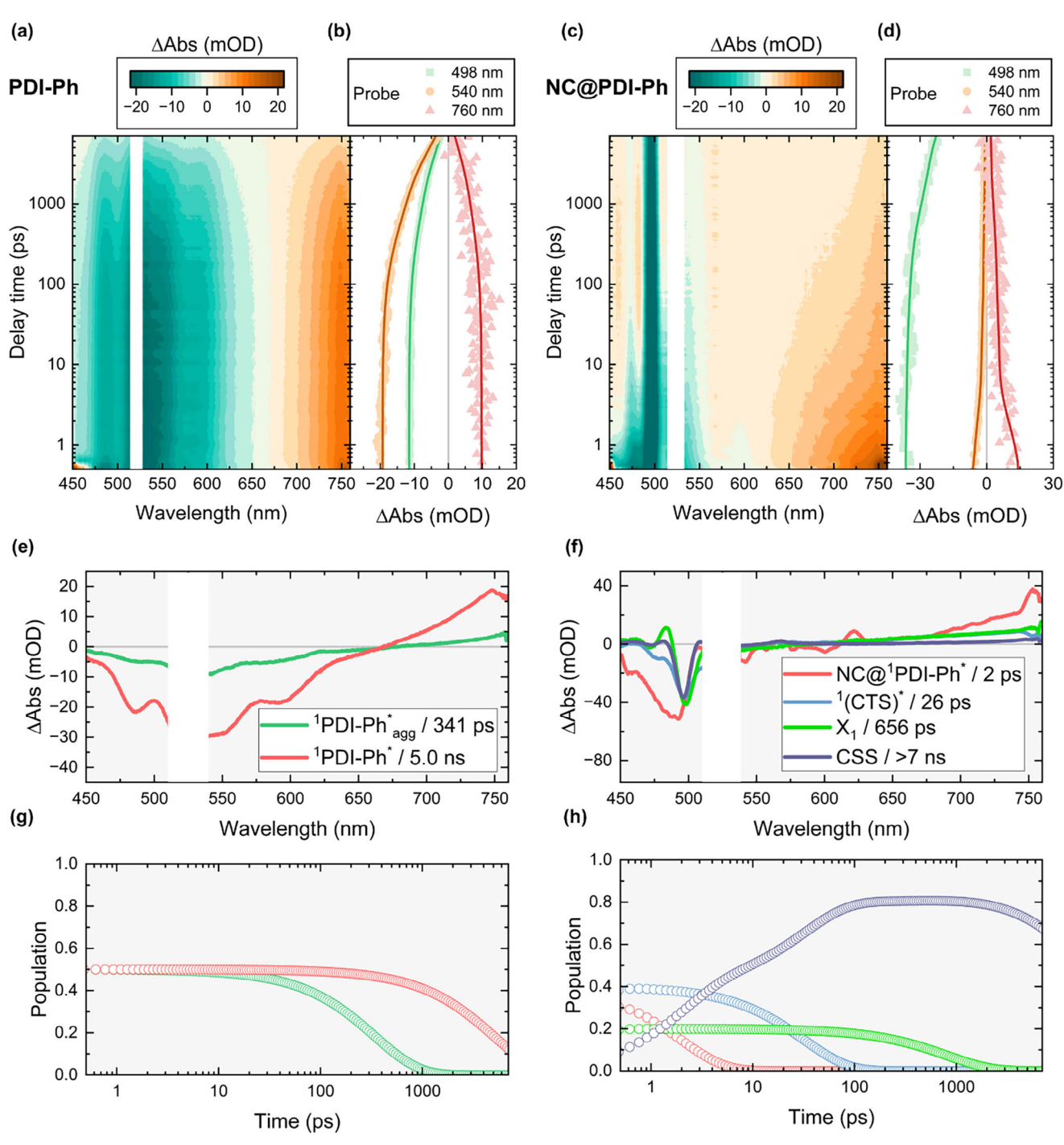


Figure 3. fs-TAS under 525 nm pump excitation. 2D pseudocolor plot for a) PDI-Ph and c) NC@PDI-Ph. Representative kinetic traces for b) PDI-Ph and d) NC@PDI-Ph. Species-associated decay spectra for e) PDI-Ph and f) NC@PDI-Ph. Relative population for g) PDI-Ph and h) NC@PDI-Ph.

are shown in (Figure 3b). Time constants for two species were determined from global target analysis (Figure 3e,g). A shorter-lived component of 341 ps and a longer-lived component of 5 ns reflect PDI-Ph aggregates (¹PDI-Ph*_{agg}) and PDI-Ph monomers (¹PDI-Ph*), respectively. For the PDI-Ph monomer, we found a lifetime that is in accordance with that obtained in TCSPC (Figure S23, Supporting Information). Similarly, PDI-PhPr also exhibits two decay components, that is, 114 ps and 4.2 ns (Figure S24, Sup-

porting Information). Here, the assignment is based on the shape of the species-associated decay spectra (SADS) for each component. Solvent-related signals interfered with the determination of the lifetimes of **PDI-Ph** and **PDI-PhPr** upon 365 nm photoexcitation in the fs-TAS, but we expect similar results.

Moving on to NC@PDI-Ph, which we photoexcited at 525 nm, striking differences were appreciated in the 2D pseudocolor maps (Figure 3c) when compared to PDI-Ph. Short-lived PDI-Ph





www.advopticalmat.de

signatures along with the concomitant appearance of a strong XB feature of NC are noted (Figure 3d). Three exponentially decaying species together with an infinite offset were needed in the target analysis of the raw data (Figure 3f,h). The corresponding lifetimes are 2 ps, 26 ps, 656 ps, and >7 ns. Relevant is the fact that the PDI-Ph singlet excited state of NC@PDI-Ph (NC@1PDI-Ph*), a charge-transfer state (CTS), and a NC-centered X1 were all initially populated. The differential spectrum of NC@1PDI-Ph* was similar to that seen for the PDI-Ph reference. In contrast, the differential absorption spectrum of the CTS included XB contributions from NC and GSB contributions from PDI-Ph. Both of them, that is, NC@1PDI-Ph* and CTS were found to undergo charge separation in 2 and 26 ps, respectively. In turn, they generate a long-lived (> 7 ns) charge-separated state (CSS), which features XB contributions from NC and a characteristic PDI •- ESA at 765 nm. The PDI• spectral features are unequivocal evidence for a charge separation that occurred upon photoexcitation. X1, which reveals a shorter lifetime than NCs on their own, also underwent charge separation in 656 ps. Upon 365 photoexcitation of NC@PDI-Ph, the fs-TA analyses afforded six species. HX, MX, and XX as the first three species are all NC-centered with lifetimes of 1, 6, and 27 ps. Relative to the observations made with the NC control, neither spectroscopic nor kinetic differences are appreciated for HX, MX, and XX. For X1 and X2, however, their lifetimes are significantly impacted. They are shortened to 52 ps and 1.8 ns, respectively. Taking the latter together with TCSPC results, we postulate that charge separation evolves from all bright excitons (Figure \$25, Supporting Information). A strong and persistent XB feature is apparent in the kinetic traces; this long-lived component (CSS) was further confirmed by ns-TAS (vide infra).

At first glance, the NC@PDI-PhPr dynamics (Figure S26, Supporting Information) under 525 nm photoexcitation involve also the growth of the XB feature at 498 nm. But, this occurred on a longer timescale than what was concluded for NC@PDI-Ph. Overall, charge separation in NC@PDI-PhPr is apparently slowed down relative to NC@PDI-Ph and we make the longer spacer responsible for that. Target analysis identified four species with lifetimes of 52 ps, 502 ps, 4.6 ns, and >7 ns. The initially populated NC@1PDI-PhPr* undergoes charge separation within 52 ps, resulting in a long-lived (> 7 ns) CSS. Accordingly, the charge-separation rate constants are $1.9 \times 10^{10} \text{ s}^{-1}$ for NC@PDI-PhPr and 5.0×10^{11} s⁻¹ for NC@PDI-Ph.^[28] Likewise, slower was the charge separation from X1 with 8.3×10^9 s⁻¹ in NC@PDI-PhPr (Figure S28, Supporting Information) than $1.9 \times 10^{10} \text{ s}^{-1}$ in NC@PDI-Ph (Figure S25, Supporting Information) under 365 nm photoexcitation. Altogether, photoexcitation of NC@PDIs at either 525 or 365 nm, consistently leads to the formation of CSSs. The shorter spacer in NC@PDI-Ph facilitates a faster charge separation, attributed to stronger intercomponent interactions.

2.4. Probing Charge Recombination in Perovskite Nanocrystal-Perylenediimide Hybrids

When inspecting the ns-TAS recorded for **NC**, the XB features decayed via ground–state recovery within 20–30 ns (Figure \$29, Supporting Information). The lifetimes are only 1.1 ns for X1 and 4.8 ns for X2 under 525 nm photoexcitation. However, photoexci-

tation at 365 nm gives rise to components X2 and X3, exhibiting lifetimes of 2.6 and 6.6 ns, respectively. Minor contributions from trap states, X(T), evolved when NC was photoexcited at 365 nm unlike that under 525 nm. X(T) are characterized by an XB feature that is persistent for 225 ns (Figure \$30, Supporting Information). For PDI-Ph upon 525 nm photoexcitation, ground state recovery was completed within 20 ns (Figure 4a,b). As a matter of fact, target analysis of the ns-TA data revealed a single decay component with a lifetime of 5 ns (Figure 4e,g). A similar behavior is observed for PDI-PhPr either upon 525 nm (Figure S31, Supporting Information), with a lifetime of 5 ns. In stark contrast, in NC@PDI-Ph the spectral features under 525 nm photoexcitation, which correspond to the XB from NC and the characteristic 765 nm ESA from (PDI•-), are even discernible on the microsecond timescale (Figure 4c). This is in sound agreement with previous reports on the PDI^{•-}, [15,29] but it is noteworthy that CSSs in NC@PDIs are significantly longer-lived compared to previous reports involving perovskite NPLs and PDI hybrids.[15,16] Nevertheless, CSS lifetimes exceeding 100 us have been reported using Rhodamine 6G (Rh6G) and non-confined CsPbI₃ NCs as electron donor and acceptor, respectively, [7aa] and up to a dozen days under ambient conditions involving non-confined CsPbBr₃ NCs and benzoquinone (BO).[30]

Remarkably, the decay of the XB feature follows a multiexponential behavior (Figure 4d), which prompts to a complex relaxation pathway. Target analysis of the ns-TA data resulted for NC@PDI-Ph in four components (Figure 4f,h). Three different charge-separated states, all featuring the PDI • fingerprint in the form of the 765 nm ESA,[15,29] were identified with lifetimes of 93 ns (CSS 1), 1.7 μs (CSS 2), and 34 μs (CSS 3). In our kinetic model, all CSSs include electrons that are localized on PDI, while the holes, which initially are generated at the NC surface, migrate across the **NC** to different traps in a sequential manner.^[31] Target analysis for NC@PDI-PhPr under 525 nm photoexcitation (Figure S32, Supporting Information) using the same model afforded lifetimes of 330 ns (CSS 1), 6.7 µs (CSS 2), and 63 µs (CSS 3).[32] Solvent-related issues interfered with the determination of the lifetimes of PDIs and NC@PDI upon 365 nm photoexcitation in the ns-TAS. All in all, we infer that the dynamics are similar across the various CSS in NC@PDI under both 525 and 365 nm. All time constants obtained from fs-and ns-TAS are found in Tables S2 and S3 (Supporting Information).

2.5. Proposed Kinetic Model

All pathways are illustrated in the Jablonski diagram of **Figure 5a**. Similar time constants are obtained for HX, MX, and XX in both systems under 365 nm excitation. It indicates that the spacer lacks an appreciable influence on the early exciton dynamics. The bright excitonic X1, X2, and X3 exhibit differences, with decay dynamics that are faster for the shorter spacer (phenyl) relative to the longer spacer (phenylpropyl). In stark contrast, under 525 nm excitation, S_1 of PDI is quenched to a variable degree, that is, faster in the presence of the shorter spacer. Additionally, a distinct charge-transfer state is detected. The quenching of these excited states results in the formation of three different charge-separated states (CSS), namely CSS1, CSS2, and CSS3, which arise from different charge location sites within the nanocrystal, whose

www.advopticalmat.de

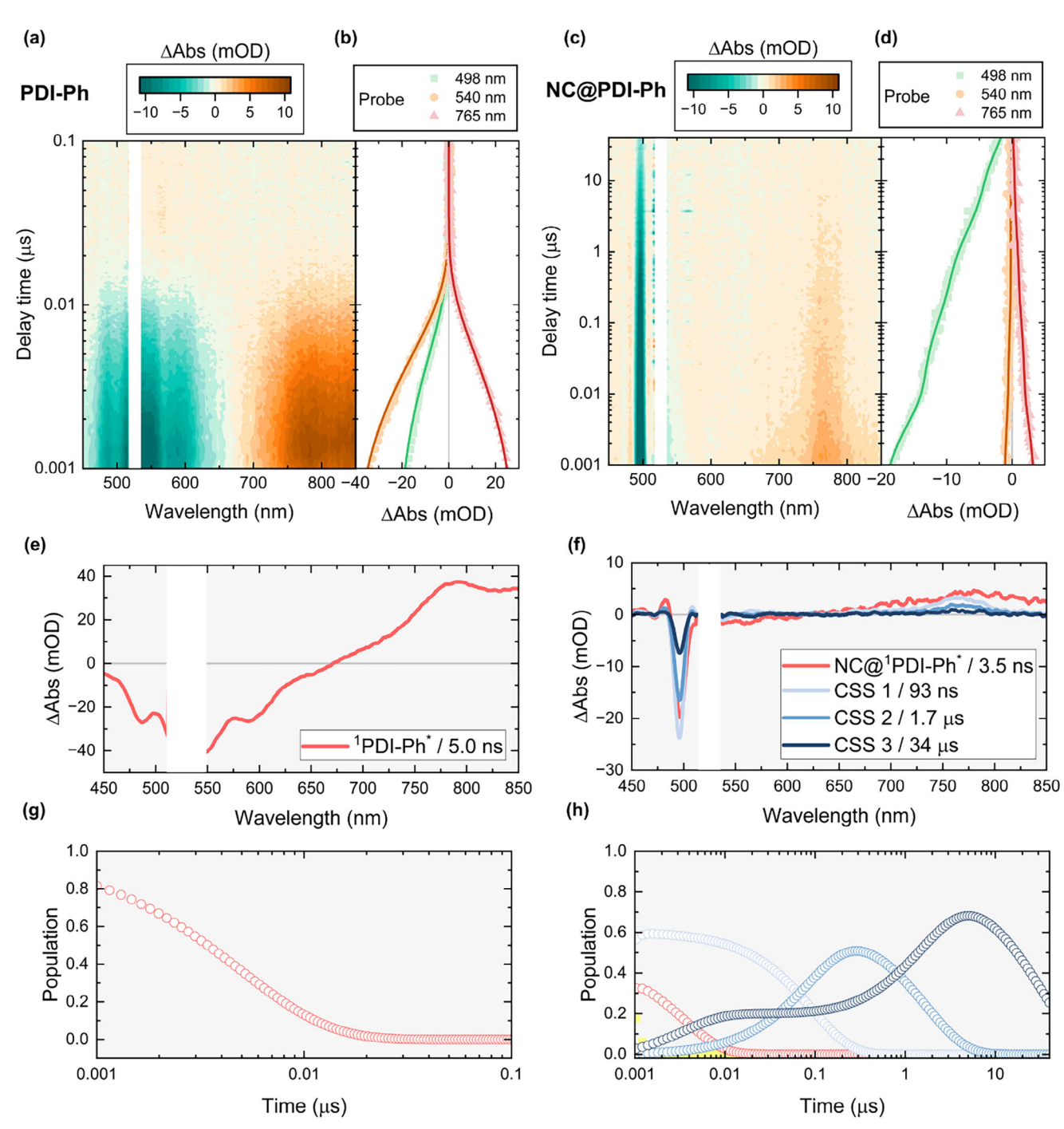


Figure 4. ns-TAS under 525 nm pump excitation. 2D pseudocolor plot for a) PDI-Ph and c) NC@PDI-Ph. Representative kinetic traces for b) PDI-Ph and d) NC@PDI-Ph. Species-associated decay spectra for e) PDI-Ph and f) NC@PDI-Ph. Relative population for g) PDI-Ph and h) NC@PDI-Ph.

lifetimes also display a clear spacer-length dependence (Figure 5b). Importantly, charge separation in NC@PDI-Ph occurred more than one order of magnitude faster under selective photoexcitation of PDI at 525 nm than under selective photoexcitation of the NC at 365 nm. Nevertheless, this difference is more subtle in the case of NC@PDI-PhPr, where charge-separation rate is about two times faster when photoexciting PDI rather than NC. Treating the charge separation

rate constant for electrons/holes as a function of spacer distance revealed significant differences (Figure S33, Supporting Information). Under 525 nm photoexcitation, charge transfer proceeded via a super-exchange mechanism through the spacer, in which the carrier tunneled quantum mechanically across the energy barrier imposed by the bridging molecule connecting the donor and acceptor. This trend is evident for when **PDI** is selectively photoexcited, while it is more challenging to

21951071, 2025, 28, Downloaded from https://ad

Figure 5. a) General kinetic model illustrating NC and PDI systems under the two excitation wavelengths used during the present work indicating the time constants determined from global target analysis for the different components. Energy shown without scaling. b) Sketch for the evolution of the charge-separated states during the proposed kinetic model.

0.0.0.0.0

(3) charge migration

rationalize it in the case of selective photoexcitation of **NC**. Here, we consider differences in the initial state delocalization within the NC conduction band.^[29] Variations in electron wavefunction overlap and the extent of delocalization is likely to influence the efficiency of a super-exchange mechanism and, in turn, to cause deviations from the expected distance dependence. Slight differences in driving force might be another plausible explanation. For example, from the energy levels of both components, a driving force of -0.7 eV is associated with an electron transfer from the CBM of the NC to the PDI LUMO, whereas a driving force of −0.5 eV is linked to a hole transfer from the PDI HOMO to the VBM of the NC. It is important to note that all of these driving forces should only be considered as estimates due to the significant uncertainties in delocalizing charge carriers within NCs. The former proceeds at a greater thermodynamic driving force, but it might well be placed within the Marcus inverted region, where an excess driving force leads to slower charge separation rates.^[33] However, it is unlikely that this mechanism is at play in semiconductor quantum dots, since Auger-assisted processes can circumvent the limitations of the inverted Marcus region by channeling excess energy into intraband excitations, instead of relying on interactions with vibrational modes.^[34] A

(2) charge separation

similar finding was recently reported for perovskite NPL-PDI when employing amino-functionalized PDIs.^[15] It is, however, important to note that different anchoring and dimensionality of the perovskites might play a different role.

(3) charge migration

A remarkable feature of NC@PDI-Ph and NC@PDI-PhPr is the exceptionally long-lived charge-separated states, especially when compared to most perovskite systems known to this date, with the exception of a few examples aforementioned. [7aa,30] Although NC@PDI-Ph exhibits an ultrafast charge separation, NC-PDI-PhPr yields longer-lived CSSs, which renders them perfect candidates for light-driven redox catalysis.

3. Conclusion

The combination of time-resolved spectroscopic techniques and kinetic analysis in a time window from femto- to microseconds were crucial to evaluate the charge separation dynamics in NC@PDIs. Interactions between the perovskite NCs and PDIs bearing carboxylic acid anchoring groups with spacers of different lengths led to efficient separation, with a rate constant 25 times faster for NC@PDI-Ph compared to NC@PDI-PhPr hybrids under selective photoexcitation to the PDI at 525 nm.

21951071, 2025, 28, Downloaded from https://advanced

ADVANCED
OPTICAL
MATERIALS

www.advopticalmat.de

Independently of the excitation wavelength, three distinct charge-separation states were populated, with lifetimes ranging from 93 ns to 34 µs for NC@PDI-Ph and from 330 ns to 63 µs for NC@PDI-PhPr hybrids. These CSS lifetimes were much longer than those reported for other perovskite-PDI systems to date, including perovskite nanoplatelets (NPLs). These findings highlight the key role of the perovskite dimensionality (NCs vs NPLs), the nature of the anchoring group and the length of the spacer between the NC and the organic acceptor molecules in the charge transfer process. A short spacer favors the interactions between the electron donors and acceptors, increasing the rates of charge separation but also the rate of charge recombination. A longer spacer led to a longer-lived CSS, which is highly desired for photovoltaic and photocatalytic applications.

4. Experimental Section

Time-Correlated Single Photon Counting Analysis: The data is fitted to a multiexponential decay function:

$$I(t) = B_1 e^{(-t/\tau_1)} + B_2 e^{(-t/\tau_2)} + B_3 e^{(-t/\tau_3)}$$
(1)

where τ_i and B_i are the lifetime and amplitude, respectively as fitting parameters of the *ith* exponential component.

The intensity average lifetime value is calculated according to:

$$\tau_{a\nu} = \frac{\sum_{i=1}^{n} B_{i} \tau_{i}^{2}}{\sum_{i=1}^{n} B_{i} \tau_{i}}$$
 (2)

The relative emission intensity is calculated as follows:

$$B_1(\%) = \frac{B_1 \tau_1}{\sum_{i=1}^n B_i \tau_i} \times 100 \tag{3}$$

Transient Absorption Data Analysis: To analyze the transient absorption data, a well-established procedure was followed. [35] First, singular value decomposition (SVD) and global analysis were performed using an all-sequential/parallel decay model. This approach yields evolution-associated spectra (EAS)/decay-associated spectra (DAS), which help determine the minimum number of kinetic components involved in the cascade. However, it is important to note that EAS/DAS do not necessarily correspond to spectra of distinct chemical species with clear physicochemical meaning. Therefore, as a second step, target analysis was applied using specific kinetic models based on plausible physical and chemical assumptions. This yields species-associated difference spectra (SADS), which represent the actual transient species involved in the photophysical processes. All data analyses, including SVD, global fitting, and target modeling, were conducted using the R-package TIMP and its graphical interface GloTarAn. [35,36]

Supporting Information

Supporting Information is available from the Wiley Online Library or from the author.

Acknowledgements

A.C.V. thanks to the "María de Maeztu" Programme for Units of Excellence in R&D (CEX 2019-000919-M) for a predoctoral fellowship (PRE2018-084294) funded by MCIN/AEI/10.13039/501100011033. A.C. is a member of the scientific staff of CIC-CONICET. The authors

gratefully acknowledge the funding by the "Solar Energy goes Hybrid" Initiative of the Bavarian Ministry for Science, Culture, and Education (SolTech) and the Deutsche Forschungsgemeinschaft for funding CRC 1719. The authors also acknowledge Grant PID2022-140315NB-100 funded by MICIU/AEI/10.13039/501100011033 and by ERDF/EU. This work was supported by Generalitat Valenciana (IDIFEDER/2018/064, IDIFEDER/2021/064, CIPROM/2022/57 and CIPROM/2021/059). It formed part of the Advanced Materials program (MFA/2022/051 and MFA/2022/028) and was supported by MCIN with funding from European Union NextGenerationEU (PRTR-C17.I1) and by Generalitat Valenciana.

Conflict of Interest

The authors declare no conflict of interest.

Data Availability Statement

The data that support the findings of this study are available from the corresponding author upon reasonable request.

Keywords

charge recombination, charge separation, colloidal perovskite nanocrystals, hybrids, perylenediimides

Received: April 14, 2025 Revised: July 15, 2025 Published online: August 5, 2025

- [1] A. Dey, J. Ye, A. De, E. Debroye, S. K. Ha, E. Bladt, A. S. Kshirsagar, Z. Wang, J. Yin, Y. Wang, L. N. Quan, F. Yan, M. Gao, X. Li, J. Shamsi, T. Debnath, M. Cao, M. A. Scheel, S. Kumar, J. A. Steele, M. Gerhard, L. Chouhan, K. Xu, X.-G. Wu, Y. Li, Y. Zhang, A. Dutta, C. Han, I. Vincon, A. L. Rogach, et al., ACS Nano 2021, 15, 10775.
- [2] L. De Trizio, I. Infante, L. Manna, Acc. Chem. Res. 2023, 56, 1815.
- [3] L. Protesescu, S. Yakunin, M. I. Bodnarchuk, F. Krieg, R. Caputo, C. H. Hendon, R. X. Yang, A. Walsh, M. V. Kovalenko, *Nano Lett.* 2015, 15, 3692.
- [4] a) J. De Roo, M. Ibáñez, P. Geiregat, G. Nedelcu, W. Walravens, J. Maes, J. C. Martins, I. Van Driessche, M. V. Kovalenko, Z. Hens, ACS Nano 2016, 10, 2071; b) N. Fiuza-Maneiro, K. Sun, I. López-Fernández, S. Gómez-Graña, P. Müller-Buschbaum, L. Polavarapu, ACS Energy Lett. 2023, 8, 1152.
- [5] a) J. T. DuBose, P. V. Kamat, Chem. Rev. 2022, 122, 12475; b) M. Palabathuni, S. Akhil, R. Singh, N. Mishra, ACS Appl. Nano Mater. 2022, 5, 10097.
- [6] K. Wu, G. Liang, Q. Shang, Y. Ren, D. Kong, T. Lian, J. Am. Chem. Soc. 2015, 137, 12792.
- [7] a) P. Maity, J. Dana, H. N. Ghosh, J. Phys. Chem. C 2016, 120, 18348;
 b) S. Sarkar, V. K. Ravi, S. Banerjee, G. R. Yettapu, G. B. Markad, A. Nag, P. Mandal, Nano Lett. 2017, 17, 5402; c) Y.-X. Zhang, H.-Y. Wang, Z.-Y. Zhang, Y. Zhang, C. Sun, Y.-Y. Yue, L. Wang, Q.-D. Chen, H.-B. Sun, Phys. Chem. Chem. Phys. 2017, 19, 1920; d) A. De, N. Mondal, A. Samanta, J. Phys. Chem. C 2018, 122, 13617; e) H. Lu, X. Zhu, C. Miller, J. San Martin, X. Chen, E. M. Miller, Y. Yan, M. C. Beard, J. Chem. Phys. 2019, 151, 204305; f) S. Mandal, L. George, N. V. Tkachenko, Nanoscale 2019, 11, 862; g) X. Luo, G. Liang, J. Wang, X. Liu, K. Wu, Chem. Sci. 2019, 10, 2459; h) J. T. DuBose, P. V. Kamat, J. Phys. Chem. Lett. 2019, 10, 6074; i) K. Wang, H. Lu, X. Zhu, Y. Lin, M. C. Beard, Y. Yan, X. Chen, ACS Energy Lett. 2020, 5,



www.advopticalmat.de

[16] Z. Wei, J. T. Mulder, R. K. Dubey, W. H. Evers, W. F. Jager, A. J. Houtepen, F. C. Grozema, J. Phys. Chem. C 2023, 127, 15406.

- [17] A. Cortés-Villena, D. Bellezza, C. Cunha, I. Rosa-Pardo, Á. Seijas-Da Silva, J. Pina, G. Abellán, J. S. Seixas de Melo, R. E. Galian, J. Pérez-Prieto, J. Am. Chem. Soc. 2024, 146, 14479.
- [18] F. J. Céspedes-Guirao, L. Martín-Gomis, K. Ohkubo, S. Fukuzumi, F. Fernández-Lázaro, Á. Sastre-Santos, Chem., A Eu. J. 2011, 17, 9153.
- [19] M. C. R. Delgado, E.-G. Kim, D. A. d. S. Filho, J.-L. Bredas, J. Am. Chem. Soc. 2010, 132, 3375.
- [20] A. Cortés-Villena, D. A. Caminos, R. E. Galian, J. Pérez-Prieto, Adv. Opt. Mater. 2023, 11, 2300138.
- [21] This ensures a sufficient number of electron acceptors in solution. Note: the PDI-C4 was injected from a stock solution in THF into the NC dispersion in toluene. A mixture of THF:DMF (95:5) in the case of PDI-C1.
- [22] Responsible is, besides a stronger deactivation in NC@PDI-C1, residual free PDI-C4, which was independently confirmed by transient absorption spectroscopy – vide infra.
- [23] V. K. Ravi, G. B. Markad, A. Nag, ACS Energy Lett. 2016, 1, 665.
- [24] A. Cortés-Villena, A. Cadranel, K. Azizi, T. Torres, D. M. Guldi, J. Pérez-Prieto, R. E. Galian, Adv. Sci. 2025, 12, 2414831.
- [25] Control experiments with a PDI reference lacking any anchor (PDI-C0) revealed negligible excited-state interactions (Figure S19). This finding underlines the key role of the anchor to enable interfacial charge separation.
- [26] The concentration of both systems was proportionally increased by 15 times for TA measurements but maintaining the same ratio of 30:1 and using 0.2 cm optical pathlength quartz cuvettes.
- [27] a) J. Li, L. Gan, Z. Fang, H. He, Z. Ye, J. Phys. Chem. Lett. 2017, 8, 6002; b) J. Kline, S. Gallagher, B. F. Hammel, R. Mathew, D. M. Ladd, R. J. E. Westbrook, J. N. Pryor, M. F. Toney, M. Pelton, S. Yazdi, G. Dukovic, D. S. Ginger, Nano Lett. 2025, 25, 5063; c) W. Zhang, Y. Ye, C. Liu, J. Wang, J. Ruan, X. Zhao, J. Han, Adv. Opt. Mater. 2021, 9, 2001885; d) H. He, Q. Yu, H. Li, J. Li, J. Si, Y. Jin, N. Wang, J. Wang, J. He, X. Wang, Y. Zhang, Z. Ye, Nat. Commun. 2016, 7, 10896.
- [28] A closer look reveals an additional species in the form of free PDI-C4 in solution, stemming from a lower K_{app} and a better solubility in toluene compared to PDI-C1 (see SI).
- [29] N. Gorczak, S. Tarkuç, N. Renaud, A. J. Houtepen, R. Eelkema, L. D. A. Siebbeles, F. C. Grozema, J. Phys. Chem. A 2014, 118, 3891.
- [30] L. Cheng, R. Hu, M. Jiang, Y. Men, Y. Wang, J. Li, T. Jia, Z. Sun, D. Feng, Nano Res. 2024, 17, 10649.
- [31] A small fraction of the excited-state population corresponding to free PDI-C1 was also noted.
- [32] The singlet excited state of free PDI-C4 decays with 4.6 ns.
- [33] R. A. Marcus, N. Sutin, Biochim. Biophys. Acta, Rev. Bioenerg. 1985, 811, 265.
- [34] a) H. Zhu, Y. Yang, K. Wu, T. Lian, Annu. Rev. Phys. Chem. 2016, 67, 259; b) H. Zhu, Y. Yang, K. Hyeon-Deuk, M. Califano, N. Song, Y. Wang, W. Zhang, O. V. Prezhdo, T. Lian, Nano Lett. 2014, 14, 1263.
- [35] I. H. M. van Stokkum, D. S. Larsen, R. van Grondelle, Biochim. Biophys. Acta, Bioenerg. 2004, 1657, 82.
- [36] a) J. J. Snellenburg, S. Laptenok, R. Seger, K. M. Mullen, I. H. M. van Stokkum, J. Statist. Softw. 2012, 49, 1; b) K. M. Mullen, I. H. M. van Stokkum, J. Statist. Softw. 2007, 18, 1.

566; j) A. De, S. Das, A. Samanta, ACS Energy Lett. 2020, 5, 2246; k) J. T. DuBose, P. V. Kamat, J. Phys. Chem. C 2020, 124, 12990; I) S. Akhil, V. G. V. Dutt, R. Singh, N. Mishra, J. Phys. Chem. C 2021, 125, 22133; m) G. Ghosh, K. Marjit, S. Ghosh, A. Ghosh, R. Ahammed, A. De Sarkar, A. Patra, J. Phys. Chem. C 2021, 125, 5859; n) S. Akhil, V. G. V. Dutt, N. Mishra, Nanoscale Adv. 2021, 3, 2547; o) S. Singh, D. Mittal, V. Gurunarayanan, A. Sahu, R. Ramapanicker, V. Govind Rao, J. Mater. Chem. A 2022, 10, 21112; p) A. Panigrahi, A. Kumar, L. Mishra, P. Dubey, S. Dutta, P. Parida, M. K. Sarangi, J. Chem. Phys. 2023, 159, 184704; g) A. Kipkorir, X. Jin, H. Gao, P. V. Kamat, J. Chem. Phys. 2023, 158, 144702; r) B. M. Sachith, Z. Zhang, P. Subramanyam, C. Subrahmanyam, A. Furube, N. Tamai, T. Okamoto, H. Misawa, V. Biju, Nanoscale 2023, 15, 7695; s) J. T. DuBose, P. V. Kamat, J. Am. Chem. Soc. 2023, 145, 4601; t) M. Ahlawat, S. Kumari, V. Govind Rao, I. Mater. Chem. A 2023, 11, 13289; u) S. Biswas, S. Akhil, N. Kumar, M. Palabathuni, R. Singh, V. G. V. Dutt, N. Mishra, J. Phys. Chem. Lett. 2023, 14, 1910; v) S. Singh, D. Mittal, V. Gurunarayanan, A. Sahu, R. Ramapanicker, V. G. Rao, ACS Appl. Energy Mater. 2023, 6, 8091; w) D. Venkateswarlu, T. Swetha, S. Akhil, M. Palabathuni, N. Mishra, S. P. Singh, Mater. Adv. 2023, 4, 1935; x) C. Du, J. Sheng, F. Zhong, Y. He, H. Liu, Y. Sun, F. Dong, Proc. Natl. Acad. Sci. U. S. A 2024, 121, 2315956121; y) A. S. Kshirsagar, K. A. Koch, A. R. Srimath Kandada, M. K. Gangishetty, JACS Au 2024, 4, 1229; z) A. Panigrahi, A. Kumar, L. Mishra, P. Parida, M. K. Sarangi, J. Phys. Chem. C 2024, 128, 17503; aa) P. Maity, R. Naphade, L. Gutiérrez-Arzaluz, S. Nematulloev, S. Thomas, W. J. Mir, K. E. Yorov, H. N. Alshareef, O. M. Bakr, O. F. Mohammed, Adv. Opt. Mater. 2024, 12, 2300941; ab) P. Sarkar, A. Sen, A. Dutta, R. Kumar, P. Sen, J. Phys. Chem. C 2025, 129, 1252. ac) M. Mukherjee, A. Chemmangat, P. V. Kamat, ACS Nano 2025, 19, 10549

- [8] a) H. Zhu, N. Song, T. Lian, J. Am. Chem. Soc. 2010, 132, 15038; b)
 T. X. Ding, J. H. Olshansky, S. R. Leone, A. P. Alivisatos, J. Am. Chem. Soc. 2015, 137, 2021; c) X. Li, Z. Huang, R. Zavala, M. L. Tang, J. Phys. Chem. Lett. 2016, 7, 1955; d) Z. Huang, Z. Xu, T. Huang, V. Gray, K. Moth-Poulsen, T. Lian, M. L. Tang, J. Am. Chem. Soc. 2020, 142, 17581
- [9] a) E. Sundin, M. Abrahamsson, Chem. Commun. 2018, 54, 5289; b)
 A. Reynal, J. Willkomm, N. M. Muresan, F. Lakadamyali, M. Planells,
 E. Reisner, J. R. Durrant, Chem. Commun. 2014, 50, 12768.
- [10] a) C. Huang, S. Barlow, S. R. Marder, J. Org. Chem. 2011, 76, 2386;
 b) N. Zink-Lorre, E. Font-Sanchis, Á. Sastre-Santos, F. Fernández-Lázaro, Chem. Commun. 2020, 56, 3824;
 c) P. Cheng, X. Zhao, X. Zhan, Acc. Mater. Res. 2022, 3, 309;
 d) X. Ran, M. A. Ali, Z. Hu, P. Li, Y. Xia, H. Zhang, L. Yang, Y. Chen, J. Phys. Chem. C 2023, 127, 5114.
- [11] J. M. Alzola, N. A. Tcyrulnikov, P. J. Brown, T. J. Marks, M. R. Wasielewski, R. M. Young, J. Phys. Chem. A 2021, 125, 7633.
- [12] X. Zhan, Z. a. Tan, B. Domercq, Z. An, X. Zhang, S. Barlow, Y. Li, D. Zhu, B. Kippelen, S. R. Marder, J. Am. Chem. Soc. 2007, 129, 7246.
- [13] A. Rossi, M. B. Price, J. Hardy, J. Gorman, T. W. Schmidt, N. J. L. K. Davis, J. Phys. Chem. C. 2020, 124, 3306.
- [14] N. Kubo, M. Yamauchi, H. Yamada, S. Masuo, J. Phys. Chem. C 2024, 128, 4648.
- [15] M. C. Gélvez-Rueda, M. B. Fridriksson, R. K. Dubey, W. F. Jager, W. van der Stam, F. C. Grozema, Nat. Commun. 2020, 11, 1901.